A theoretical study of the interactions of NF_3 with neutral ambidentate electron donor and acceptor molecules†

Fernando Blanco,*[a] Ibon Alkorta,[b] Isabel Rozas,[a] Mohammad Solimannejad[c] and José Elguero[b]

Received 12th April 2010, Accepted 22nd September 2010
DOI: 10.1039/c0cp00199f

A theoretical study of the complexes (dimers and trimers) formed between nitrogen trifluoride (NF_3) and the ambidentate electron donor/acceptor systems HF, FCl, HCN, and HNC has been carried out using DFT [M05-2x/6-311++G(d,p)] and *ab initio* methods [(MP2/6-311++G(d,p) and MP2/aug-cc-pVTZ)]. Due to its structure, the NF_3 molecule can interact with both electron acceptors and electron donors through its N and F atoms. Thus, five minimum energy structures have been located for the dimers and four minima structures have been studied for the trimer complexes. New σ-hole bonding complexes have been located.

Introduction

Nitrogen trifluoride (NF_3) is a colourless, toxic, odourless, non-flammable gas, employed in the electronics industry, particularly in the manufacture of liquid crystal screens. It was first discovered by Ruff *et al.* in 1928,[1] and its structure, bonding, and molecular properties have been extensively studied for many years.[2] During long time it was considered that its industrial use was safe because, compared to other fluorinated compounds (CF_4 and C_2F_6), NF_3 shows shorter atmospheric lifetime and does not produce carbon contamination residues. Hence, the industrial use of NF_3 as a substitute for other perfluorinated gases remarkably increased during the last decade,[3] resulting in a very large amount of NF_3 atmospheric emissions. In fact, between 1978 and 2008 an increment of 11% per year of NF_3 emissions was recorded.[4] However, recent studies are warning that, even though NF_3 is not included within the list of greenhouse gasses of the Kyoto protocol,[5] there is a clear risk in using NF_3 because its effects as a greenhouse gas are much longer than other recognized contaminants as CO_2.[6]

The interactions between NF_3 and different chemical species have been previously studied both computationally and experimentally. In a thorough study, Antoniotti, Grandinetti *et al.* analyzed the nature of NF_3 adsorption on solid surfaces, providing the first theoretical evidence for the behavior of NF_3 as a bifunctional Lewis base when interacting with neutral Lewis acids.[7] The interaction of NF_3 with a Si surface was studied both by X-ray photoelectron spectroscopy and by DFT calculations by the group of Ohuchi.[8] To investigate if the photodecomposition of NF_3 could compete with its reaction with the atomic oxygen atoms, O (1D), Antoniotti and Grandinetti carried out a computational study of the mechanism of such a reaction.[9] In addition, the infrared spectra of the complex of NF_3 with HF were observed in solid argon matrices,[10] and the rotational spectrum of the NF_3–ClF complex was determined by Legon and co-workers by pulsed-nozzle, Fourier transform microwave spectroscopy.[11] But probably, the interactions most extensively studied are those established between NF_3 and different cations. Thus, Antoniotti *et al.* performed the study of the gas-phase reactions of the Si^+ ions with NF_3 by quadrupole ion trap mass spectrometry and *ab initio* calculations.[12] The complexes formed between NF_3 and H^+, Li^+, Na^+ and K^+ have been computationally analyzed and they appear to form ion–dipole interactions.[13] Moreover, the structure and stability of the experimentally unknown Li^+, Mg^+ and Be^+–NF_3 ions have been theoretically investigated by Grandinetti and co-workers. They concluded that these complexes could be observed as stable species in the gas phase, supporting the idea proposed by Fujii that techniques such as Mg^+ or Li^+ ion attachment mass spectroscopy are plausible to quantify the emissions of fluorinated greenhouse gases and that they could also be employed to quantify the emissions of NF_3.[14] Consequently, a better understanding of NF_3 properties and its possible interactions has become a subject of interest, thus we present here the computational study of the complexes that this molecule can form with different chemical substances, in particular the "ambidentate" electron donor/acceptor molecules HF, FCl, HCN, and HNC.

Computational methods

The systems have been optimized at the M05-2x[15] and MP2[16] computational levels with the 6-311++G(d,p)[17] basis set. The M05-2x functional has shown to be able to describe properly weak interactions where other traditional functionals fail.[18] Frequency calculations have been performed at the same computational levels to confirm that the resulting optimized structures are energetic minima. Additionally, geometry optimizations have been performed at the MP2/aug-cc-pVTZ[19] level

[a] *School of Chemistry, University of Dublin, Trinity College, Dublin 2, Ireland. E-mail: blancof@tcd.ie; Fax: +353 1 671 2826*
[b] *Instituto de Química Médica (CSIC), Juan de la Cierva, 3, 28006-Madrid, Spain*
[c] *Quantum Chemistry Group, Department of Chemistry, Arak University, 38156-879 Arak, Iran*

† Electronic supplementary information (ESI) available: Energetic, geometric and electronic details of the computational results. Cartesian coordinates of the complexes calculated at the MP2/6-311++G(d,p) computational level. See DOI: 10.1039/c0cp00199f

for more accurate results. The interaction energy of the clusters in the present article has been calculated as the difference between the supermolecule's energy and the sum of energies of the isolated monomers in their minimum energy configuration. The interaction energy for all the complexes studied has been corrected from the inherent basis set superposition error (BSSE) using the full counterpoise method.[20]

The electron density of the isolated molecules and complexes has been analysed within the Atoms in Molecules (AIM) methodology[21] using the AIMPAC[22] and MORPHY98 programs.[23] The atomic properties have been obtained by integration within the atomic basins. The integration conditions have been modified until the integrated Laplacian value obtained for each atom is smaller, in absolute value, than 10^{-3} since previous articles have shown that these conditions assure a negligible error in the total energy and charge of the system.[24]

The Natural Bond Orbital (NBO) method[25] has been used to analyze the interaction of the occupied and unoccupied orbitals with the NBO-5 program.[26] This kind of interactions is of most importance in the formation of hydrogen bonds and other charge transfer complexes. In addition, the Natural Energy Decomposition Analysis[27] has been carried out to obtain insights of the source of the interactions. These calculations have been performed using the GAMESS program.[28]

Results and discussion

Nitrogen trifluoride (NF_3), as its structural analogue ammonia (NH_3), is a trigonal pyramidal molecule with experimental N–F bond length of 1.371 Å and F–N–F angle of 102.2°.[29] Calculated geometries with the different computational methods considered in this study are in good agreement with the gas-phase experimental data (Table 1).

Replacement of H atoms by F ones produces significant differences in the electronic properties of NF_3 compared to NH_3. The N–H bond is strongly polarized due to the different electronegativity of the atoms, thus inducing a displacement of the electronic density towards the nitrogen lone pair. The polarization of the N–F bond is lower and the displacement of the charge occurs towards the highly electronegative F atom attracting electron density of the nitrogen lone pair. Thus, NH_3 is basic and highly polar (1.420 D), while NF_3 is less basic and shows a lower dipole moment of 0.234 D[30] oriented in opposite direction (Fig. 1). Similar inversion of the electronic properties has been described in other systems due to perfluorination.[31]

The molecular electrostatic potential (MEP) of NH_3 (Fig. 2a, left side) has a simple distribution with two well differentiated areas, one negative region (yellow) corresponding to the nitrogen lone pair, and one positive region (blue), corresponding to the hydrogen atoms. In NF_3, the inclusion of three electron withdrawing fluorine atoms reduces considerably the electronic availability in the nitrogen lone pair. Thus, the MEP of NF_3 (Fig. 2a, right side) shows ten negative regions: one around the lone pair of the N atom, clearly smaller than that observed in NH_3, and nine surrounding

Table 1 Experimental and calculated geometry parameters and dipole moment of NF_3

Method	N–F/Å	F–N–F/°	Dipole/D
Experimental[31]	1.371	102.2	0.234
M05-2x/6-311++G(d,p)	1.356	102.2	0.316
MP2/6-311++G(d,p)	1.370	102.2	0.466

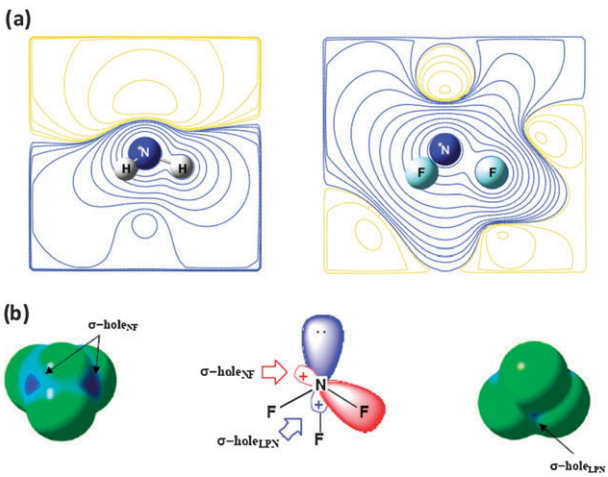

Fig. 2 (a) MEP graph sections of NH_3 (left) and NF_3 (right) calculated at MP2/6-311++G(d,p) level (isovalues represented are $\pm 20, 8 \times 10^{-n}, 4 \times 10^{-n}, 2 \times 10^{-n}$ with $n = 0, 1, 2, 3$). (b) Two different views of the NF_3 calculated MP2/6-311++G(d,p) electrostatic potential, computed on the 0.001 electrons bohr^{-3} contour of the electronic density (green and blue surfaces correspond to regions of negative and positive potential respectively). Region of potential associated to a σ-hole$_{NF}$ (left) and σ-hole$_{LPN}$ (right) are indicated.

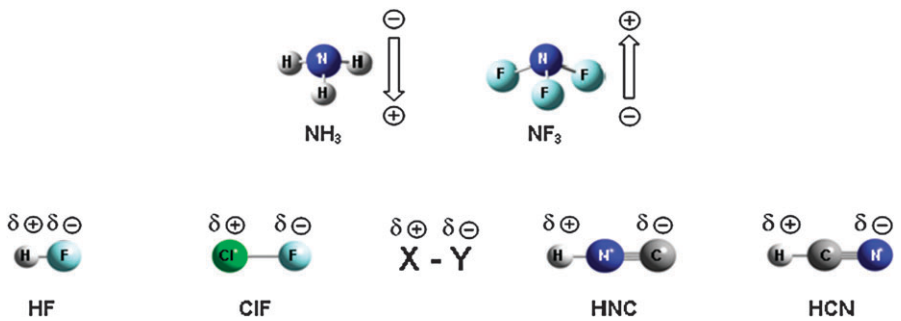

Fig. 1 Monomers studied in this work indicating dipole moment direction for NH_3 and NF_3 molecules and partial charges for the X–Y monomers chosen.

Table 2 Calculated values of the molecular electrostatic potential minima (kJ mol^{-1}) of NH_3 and NF_3 at the M05-2x/6-311++G(d,p) and MP2/6-311++G(d,p) computational levels

	NH_3		NF_3	
MEP	M05-2x/6-311++G(d,p)	MP2/6-311++G(d,p)	M05-2x/6-311++G(d,p)	MP2/6-311++G(d,p)
LP_N	−309.02	−301.67	−20.48	−22.84
LP_{Fup}	—	—	−13.65	−11.56
LP_{Fdown}	—	—	−12.60	−11.56

the F atoms. The MEP minima values of these negative regions are gathered in Table 2. They are slightly less negative for the F lone pairs than for the N lone pair.

The positive potential region in NF_3 is more delocalized than in NH_3 due to the effect caused by the presence of the F atoms. Fig. 2b shows the positions described in the literature as a σ-hole (positive region corresponding to the lobe that is not involved in a covalent σ bond), one for each N–F bond in the case of NF_3 (σ-$hole_{NF}$) (Fig. 2b, left side). These σ-holes, described by Politzer *et al.*,[32] can play a relevant role in the formation of coordinating structures. In our study, another possible *pseudo*-σ-hole has been observed. We postulate that this electron deficient region is associated to the N lone pair (σ-$hole_{LPN}$) and, even though small, it is clearly observed in the electrostatic potential computed on the electron density map (Fig. 2b, right side). All of these four positive regions are possible sites of interaction and each one could be involved in the formation of specific weak interactions with electron donating groups.

Experimental and theoretical studies had confirmed that even with neutral Lewis acids, NF_3 can behave as a bi-functional Lewis base, either by the lone pair of nitrogen or by the fluorine atoms, forming isomeric structures of comparable stability.[7] We have also revised the proton affinity (PA) of NF_3 as an additional approach to its reactivity. As it was previously reported[33] the F- and the N-protonated forms of NF_3 are distinct species in the gas phase. The global minimum corresponds to the F-protonated isomer $[NF_2–FH]^+$, which can be viewed as an ion/dipole complex. The N-protonated form $[H–NF_3]^+$ is less stable. We have calculated PA of NF_3 at MP2 level. The calculated value for the protonation on the fluorine atom $[NF_2–FH]^+$ is in good agreement with the experimental one (Table 3) and confirms that NF_3 is less basic than NH_3.

Given the interesting characteristics of NF_3, we decided to study its complexes (dimers and trimers) with different small, linear and polarized molecules (HF, ClF, HNC, HCN) that allowed us to analyze a wide variety of interactions with a reasonable computational cost.

Table 3 Calculated and experimental proton affinity (kJ mol^{-1}) of NH_3 and NF_3

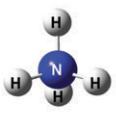

$[NH_4]^+$

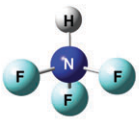

$[H\text{-}NF_3]^+$

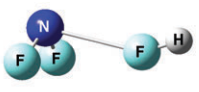

$[NF_2\text{-}FH]^+$

PA	NH_3	NF_3	
Experimental	853.7[34]	589.1[35] (568.6[34])	
MP2/6-311++G(d,p)	852.9	544.9[a]	588.4[b]

[a] Geometry $[H–NF_3]^+$. [b] Geometry $[NF_2–FH]^+$.

Dimers

Structure and energy analysis. Based on the characteristics of the monomers, five kinds of dimeric structures were considered (Fig. 3) and they were computed at three calculation levels (M05-2x/6-311++G(d,p), MP2/6-311++G(d,p) and MP2/aug-cc-pVTZ). Three of these dimers corresponded to the coordination of the negative regions of NF_3 (the N lone pair [structure **A**], or the F atoms [structures **B** and **C**]), with the electron demanding side (X) of the selected partners, and the other two corresponded to the interaction of the positive regions of NF_3 (the two described σ-holes [structures **D** and **E**]), with the electron donor side (Y) of the corresponding partners.

For any given case, the interaction values (see Table 4), although not identical, follow the same trend for the three computational methods. The correlation is lower for the M05-2x/6-311++G(d,p) method [r^2 = 0.67 with MP2/6-311++G(d,p) and r^2 = 0.59 with MP2/aug-cc-pVTZ, respectively], but much better between the two MP2 methods [MP2/6-311++G(d,p) and MP2/aug-cc-pVTZ, r^2 = 0.91]. The BSSE corrected interaction energies at the M05-2x/6-311++G(d,p) and MP2/aug-cc-pVTZ computational levels provide relative similar values while those at MP2/6-311++G(d,p) show large BSSE correction values (see Table 4).

Analysis of the interaction energies calculated with the MP2/aug-cc-pVTZ level of optimization shows that the dimers of type **A** (*NF_3 e-donor complexes* by the N lone pair) are the most favoured in the coordination with HF, ClF and HNC. The stabilization achieved is over 4 kJ mol^{-1} (HF, ClF) and 2 kJ mol^{-1} (HNC) better than **B** and **C** (3 and 2 kJ mol^{-1}, respectively, when BSSE corrected energies are considered). The dimers of type **D** (*NF_3 e-acceptor complexes* through the σ-hole associated to the N–F bond) are less stable when coordinating with HF, ClF and HNC, but relatively close to the respective absolute minimum. In the HCN series, however, the absolute minimum narrowly corresponds to the type **D** dimer. Thus, considering energetic terms, in the NF_3 : HCN complex, NF_3 should preferably act as electron acceptor by one of the N–F associated σ-holes interacting with the HCN nitrogen lone pair. Dimers of type **E** (*NF_3 e-acceptor complexes* through the σ-hole associated to the N lone pair), in all the cases, are the most unstable showing the smallest values of interaction energy.

The calculated interaction distances (*d*) are gathered in Table 5. We have found a good correlation for this parameter

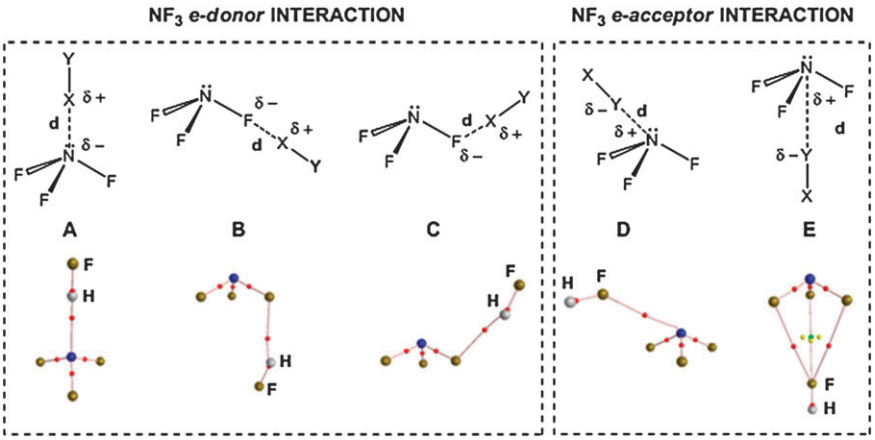

Fig. 3 General structure of the five dimers studied here (above) and molecular graph (AIM) of the NF_3 : HF complexes at the M05-2x/6-311++G(d,p) computational level (below). Red, yellow and green balls indicate bond, ring and cage critical points respectively.

Table 4 Interaction energies (without and with BSSE correction by counterpoise method **CP**) of the dimers (kJ mol^{-1})

			M05-2x/6-311++G(d,p)		MP2/6-311++G(d,p)		MP2/aug-cc-pVTZ	
XY	Comp.	PG	ΔE (no CP)	ΔE (CP)	ΔE (no CP)	ΔE (CP)	ΔE (no CP)	ΔE (CP)
HF	**A**	C_{3v}	−9.43	−5.78	−10.41	−3.62	−10.44	−6.88
HF	**B**	C_s	−7.11	−4.87	−6.42	−2.60	−6.46	−3.99
HF	**C**	C_s	−7.24	−5.29	−6.87	−2.99	−6.43	−4.06
HF	**D**	C_s	−6.61	−4.71	−4.70	−1.40	−3.80	−2.68
HF	**E**	C_{3v}	−3.46	−1.90	−2.51	1.08	−1.70	−0.89
ClF	**A**	C_{3v}	−9.90	−6.75	−9.07	−2.75	−10.44	−7.61
ClF	**B**	C_s	−6.86	−4.70	−5.40	−0.90	−6.01	−4.41
ClF	**C**	C_s	−6.09	−4.16	−5.75	−0.95	−5.68	−4.11
ClF	**D**	C_s	−6.26	−3.18	−6.32	−0.31	−5.20	−3.43
ClF	**E**	C_{3v}	−4.88	−1.57	−5.47	1.76	−3.05	−1.75
HNC	**A**	C_{3v}	−5.85	−3.41	−8.47	−3.02	−9.56	−5.61
HNC	**B**	C_s	−5.89	−4.16	−7.15	−3.07	−7.94	−4.68
HNC	**C**	C_s	−5.76	−4.25	−7.11	−3.22	−7.38	−4.31
HNC	**D**	C_s	−5.87	−4.03	−5.73	−2.57	−5.12	−3.67
HNC	**E**	C_{3v}	−2.78	−1.35	−2.16	0.15	−1.77	−0.85
HCN	**A**	C_{3v}	−3.02	−1.28	−5.36	−1.25	−5.57	−2.59
HCN	**B**	C_s	−4.19	−2.70	−5.12	−1.67	−5.38	−2.71
HCN	**C**	C_s	−3.73	−2.54	−4.72	−1.65	−4.55	−2.25
HCN	**D**	C_s	−6.71	−4.76	−6.15	−2.70	−5.99	−4.32
HCN	**E**	C_{3v}	−3.31	−1.62	−2.84	−0.06	−2.74	−1.40

among the different methods [r^2 = 0.993 M05-2x/6-311++G(d,p) *vs.* MP2/6-311++G(d,p), r^2 = 0.979 M05-2x/6-311++G(d,p) *vs.* MP2/aug-cc-pVTZ, r^2 = 0.983 MP2/6-311++G(d,p) *vs.* MP2/aug-cc-pVTZ].

In general, the distances found in the dimers **A–C** are considerably shorter than in the complexes **D–E**, that could be explained by the repulsion exerted between the interacting fluorine and the negative side of the XY partner involved in the complexation in the case of the **D–E** structures.

Electron density difference maps describe the electronic displacement produced as a result of the complexation compared to the electronic distribution in the isolated monomers. As it can be seen from Fig. 4, the NF_3 : HF complex of type **A** shows a clear charge-depleting region (yellow surface) over the non-interacting fluorine atoms of NF_3, and two significantly charge-gaining regions (blue surface), one concentrated over the N lone pair and the other on the HF subunit in the face opposite to the interaction. In the complexes of type **B** and **C** the depletion of charge is observed over the N lone pair and the non-interacting F atoms, and the increase in charge occurs over the NF_3 interacting fluorine and over the F atom of the HF subunit.

In these three cases (**A–C**) the direction of the negative charge displacement goes from NF_3 to HF, through the hydrogen bond (HB) that corresponds to a *NF_3 e-donor* behaviour. In complexes of type **D** and **E** the pattern is different, the graphical analysis is not obvious but the direction of the negative charge displacement suggests a *NF_3 e-acceptor* behaviour. A gain of negative charge is observed over the N and F lone pairs of NF_3, and a slight depletion of charge is perceived in the H of the HF subunit. In global terms, the charge-transfer is more evident in the complexes **A–C**, where the largest increase of electron density occurs clearly in the interaction area, than in the **D–E** ones.

Electron density analysis. The topological analysis of the electron density based on the AIM theory is a tool to evaluate the characteristics of covalent bonds and weak interactions.

Table 5 Interaction distances (Å) and electron density of intermolecular bcps (au) of the dimers

XY	Comp.	M05-2x/6-311++G(d,p) *d*	MP2/6-311++G(d,p) *d*	MP2/aug-cc-pVTZ *d*	M05-2x/6-311++G(d,p) ρ	M05-2x/6-311++G(d,p) $\nabla^2\rho$
HF	**A**	2.057	2.053	2.020	0.0190	0.0766
HF	**B**	2.088	2.131	2.081	0.0131	0.0589
HF	**C**	2.029	2.057	2.033	0.0146	0.0681
HF	**D**	2.849	3.026	2.992	0.0074	0.0382
HF	**E**	3.026	3.107	3.175	0.0044	0.0242
ClF	**A**	2.747	2.833	2.694	0.0178	0.0716
ClF	**B**	2.834	2.972	2.866	0.0105	0.0486
ClF	**C**	2.799	2.907	2.835	0.0114	0.0527
ClF	**D**	2.836	2.916	3.030	0.0071	0.0359
ClF	**E**	2.913	2.968	3.072	0.0058	0.0298
HNC	**A**	2.260	2.205	2.166	0.0125	0.0476
HNC	**B**	2.164	2.170	2.143	0.0106	0.0471
HNC	**C**	2.131	2.118	2.089	0.0114	0.0518
HNC	**D**	3.360	3.454	3.326	0.0046	0.0163
HNC	**E**	3.581	3.698	3.693	0.0026	0.0109
HCN	**A**	2.532	2.486	2.429	0.0077	0.0250
HCN	**B**	2.368	2.401	2.384	0.0072	0.0292
HCN	**C**	2.353	2.353	2.303	0.0072	0.0301
HCN	**D**	3.154	3.248	3.139	0.0054	0.0230
HCN	**E**	3.285	3.446	3.368	0.0039	0.0170

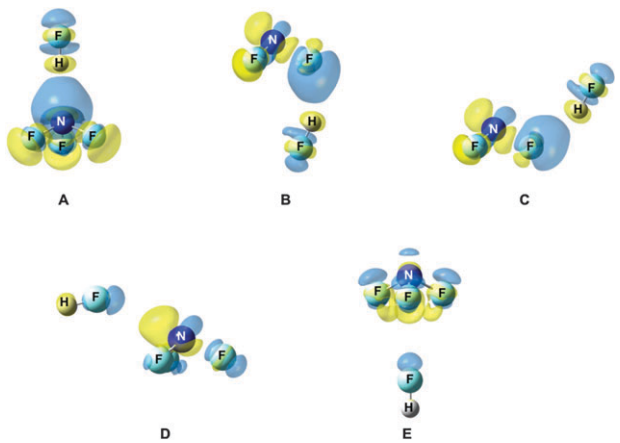

Fig. 4 Some examples of the electron density difference maps of NF_3 : HF dimers located in this work. Blue and yellow isosurfaces represent gain and loss of electron density upon complexation with respect to the isolated subunits. Contours shown are 0.0002 e per au calculated at the M05-2x/6-311++G(d,p) level.

The graphical analysis of the dimers (Fig. 3) shows the presence of an intermolecular bond critical point (bcp) in all the complexes. These bcps present small values of the electron density (ρ) and positive Laplacian ($\nabla^2\rho$) (see Table 5), an indication of the closed shell characteristics of the clusters, similar to those found in other weak interactions.[36,37] In previous works, we had described exponential relationships between the interaction distance and the electron density and Laplacian at the bcp for hydrogen-bonded systems.[38,39] Here, due to the variety of interactions, the correlation found is low (r^2 = 0.66) when considering all the dimers, but it increases considerably (r^2 = 0.90) if we only consider the complexes **A–C**, which present a more similar pattern of interaction.

Natural bond orbital analysis. A NBO analysis was performed to evaluate different electronic properties of the systems. The study of NBO charges of NF_3 in the dimers (Table 6) shows that there is a clear charge transfer in the *NF_3 e-donor complexes* **A**, and to a lesser extent in **B** and **C**, but not in the *NF_3 e-acceptor complexes* **D** and **E**. That is consistent with the description of electronic displacement discussed before.

The NBO second order perturbation energy (*E*2, Table 6) reveals an orbital interaction in dimers of type **A**, from the lone pair of the N atom of the NF_3 molecule to the antibonding orbital of the XY moiety [$LP_N \rightarrow BD^*$ XY], and in the complexes of type **B** and **C**, from the lone pair of the interacting F atom of NF_3 [$LP_F \rightarrow BD^*$ XY] to the same XY antibonding orbital. This kind of interaction is mainly responsible for the stabilization energy of the cluster and it was not observed in the complexes of type **D** or **E**. The *E*2 energy is related to the absolute interaction energy, being larger in the complexes of type **A** (the most stable ones in almost all cases), in agreement with the NBO charges and the electron density difference maps.

Natural energy decomposition analysis (NEDA) is a method for partitioning molecular interaction energies into charge transfer (CT), electrostatic (ES), polarization (POL), and intermolecular exchange component (XC). The NEDA results indicate that the main stabilization term is the charge transfer, its contribution being more significant in the complexes of type **A–C**. In terms of the NEDA analysis, and as expected, the ES is generally small and this could be explained attending to the neutral nature of the systems involved in the interactions. The polarization term only plays a significant role in the complexes of type **D** and **E**, where it is the most important component in some of the cases, and in the specific case of the ClF complexes of type **A–C**, due to the participation in the interaction of the chlorine atom, which presents a very polarized electronic cloud.

Repulsion between the cores (see ESI†) is another of the basic components in the NEDA analysis and is measured by the deformation of the electronic clouds (DEF). This kind of interaction is opposed to the bonding and, in general, has

Table 6 NBO and NEDA analysis of calculated dimers at the M05-2x/6-311++G(d,p) computational level

				Natural energy decomposition analysis (NEDA)/kJ mol^{-1}			
XY	Comp.	Charge transfer (e)[a]	E2/kJ mol^{-1}	CT	ES	POL	XC
HF	**A**	0.015	19.29	−35.61	−11.09	−3.35	−8.20
HF	**B**	0.005	8.03	−15.56	−6.19	−5.73	−7.15
HF	**C**	0.005	12.01	−16.69	−7.78	−6.44	−6.57
HF	**D**	0.001	0.00	−7.57	−6.40	−18.16	−11.34
HF	**E**	0.001	0.00	−7.49	−1.30	−12.89	−8.66
ClF	**A**	0.022	19.83	−38.33	−15.23	−35.19	−18.74
ClF	**B**	0.007	7.15	−17.28	−5.27	−23.89	−12.80
ClF	**C**	0.006	9.20	−16.78	−5.90	−25.27	−12.18
ClF	**D**	0.002	0.00	−10.96	−3.51	−11.09	−8.41
ClF	**E**	0.003	0.00	−9.25	−1.84	−9.62	−8.49
HNC	**A**	0.015	16.53	−28.91	−5.98	−3.51	−7.53
HNC	**B**	0.008	11.63	−19.71	−4.77	−5.44	−5.90
HNC	**C**	0.007	14.90	−19.83	−5.56	−6.69	−6.40
HNC	**D**	0.003	0.00	−8.58	−6.02	−8.24	−7.74
HNC	**E**	0.002	0.00	−6.95	−1.59	−5.19	−5.10
HCN	**A**	0.010	10.00	−20.08	−2.47	−2.85	−5.40
HCN	**B**	0.005	7.61	−14.56	−3.01	−5.65	−4.77
HCN	**C**	0.004	8.66	−13.05	−2.97	−5.98	−4.81
HCN	**D**	0.003	0.00	−12.13	−6.19	−15.48	−10.79
HCN	**E**	0.003	0.00	−9.54	−2.01	−9.54	−8.08

[a] Positive values mean charge transfer from NF_3 to XY in the complex.

resulted more pronounced in the case of structures with stronger interactions, in which the nuclei are closer.

Trimers

Structure and energy analysis. As it has been described, NF_3 can form complexes as *e-donor* (through the lone pairs of N and F atoms) and as *e-acceptor* (through σ-holes). In this section, we discuss this dual nature acting simultaneously with pairs of XY molecules. A variety of possible combinations was explored. For each XY : NF_3 : XY system four different minima were located which are shown in Fig. 5, none other configuration resulted stable. As depicted, in the **BD** and **CD** trimers, NF_3 acts as *e-acceptor* through the σ-hole associated to one of the N–F bonds (σ-hole$_{NF}$), and as *e-donor* through one of the F terminal atoms (with two orientations above and below the plane of fluorine respectively). In trimers of type **AE** and **CE**, NF_3 acts as *e-acceptor* through the *pseudo*-σ-hole associated to the nitrogen lone pair (σ-hole$_{LPN}$), and as *e-donor* either from the N lone pair (**AE**) or from the lone pair of one of the terminal F atoms (**CE**). In a few cases the proposed complexes are not stable and evolve to other more stable configurations as in the **CE** complexes with HCN and **CD** complexes of ClF at MP2 level.

The energetic results (Table 7) show that, in general terms, the interaction values, though not identical, follow the same trend for the three calculation levels. The correlation is very low for the M05-2x/6-311++G(d,p) (r^2 = 0.42 and r^2 = 0.15 with MP2/6-311++G(d,p) and MP2/aug-cc-pVTZ respectively) but better between the MP2/6-311++G(d,p) and MP2/aug-cc-pVTZ (r^2 = 0.80). When we consider the interaction energies of dimers and trimers together so that we have a volume of statistical data more consistent, the correlation

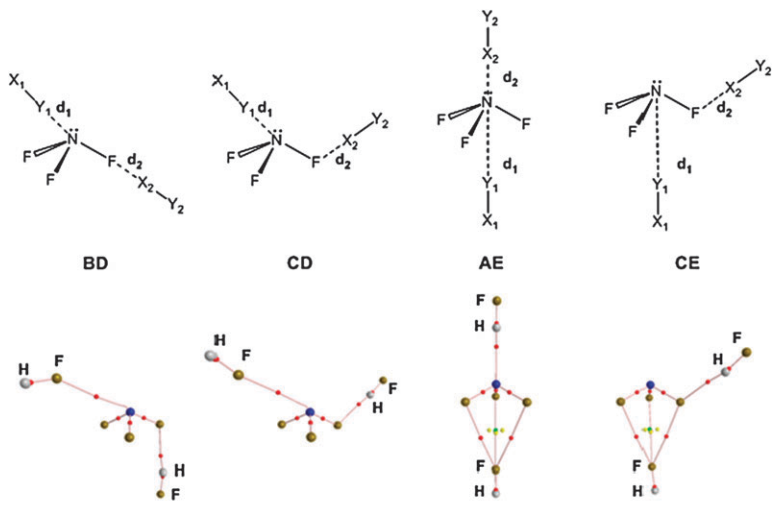

Fig. 5 General structure of the four trimers studied here (above) and molecular graph (AIM) of the HF : NF_3 : HF complexes at the M05-2x/6-311++G(d,p) computational level (below). Red, yellow and green balls indicate bond, ring and cage critical points respectively.

coefficients between the three methods improve significantly [r^2 = 0.91 M05-2x/6-311++G(d,p) *vs.* MP2/6-311++G(d,p), r^2 = 0.81 M05-2x/6-311++G(d,p) *vs.* MP2/aug-cc-pVTZ, r^2 = 0.95 MP2/6-311++G(d,p) *vs.* MP2/aug-cc-pVTZ]. As in the case of the dimers, the M05-2x/6-311++G(d,p) and MP2/aug-cc-pVTZ BSSE corrected energies provide closer values while those of the MP2/6-311++G(d,p) are significantly smaller in absolute value.

An energetic cooperativity effect has been observed and then evaluated using eqn (1),

$$\begin{aligned}\text{Coop-Energy} = {} & E_i(X_1Y_1 : NF_3 : X_2Y_2) \\ & - E_i(X_1Y_1 : NF_3) - E_i(NF_3 : X_2Y_2) \\ & - E_i(X_1Y_1 : X_2Y_2) \qquad (1)\end{aligned}$$

where $E_i(X_1Y_1 : NF_3 : X_2Y_2)$ is the interaction energy of the trimer, $E_i(X_1Y_1 : NF_3)$ and $E_i(NF_3 : X_2Y_2)$ are the interaction energies of the isolated dimers within their corresponding minima configuration, and $E_i(X_1Y_1 : X_2Y_2)$ is the interaction energy of the monomers X_1Y_1 and X_2Y_2 in the geometry they have in the trimer. The energetic results of these cooperative effects (with and without BSSE corrections) are gathered in Table 8, and in all the cases a favourable cooperativity is observed. The calculated BSSE corrected cooperative effects are smaller in absolute terms, but this correction does not affect the general trend.

A selection of the geometrical parameters of the optimized trimers has been gathered in Table 8, where d_1 and d_2 are the interaction distances indicated in Fig. 5 (d_1 corresponds to *NF_3 e-acceptor* interaction and d_2 corresponds to *NF_3 e-donor* interaction). Table 8 only presents the results obtained with the higher level of calculation for the sake of simplicity. We have found a good correlation for both interaction distances among the different methods [r^2 = 0.991 M05-2x/6-311++G(d,p) *vs.* MP2/6-311++G(d,p), r^2 = 0.973 M05-2x/6-311++G(d,p) *vs.* MP2/aug-cc-pVTZ, r^2 = 0.985 MP2/6-311++G(d,p) *vs.* MP2/aug-cc-pVTZ] (see ESI†).

The differences between the interaction distances d_1 and d_2 in the trimer less the distance for the same type of interaction in the related dimer(Δd_1 and Δd_2) are shown in Table 8. As it can be

Table 7 Interaction energies (without and with BSSE correction by counterpoise method CP) of the trimers (kJ mol^{-1})

		M05-2x/6-311++G(d,p)		MP2/6-311++G(d,p)		MP2/aug-cc-pVTZ	
XY	Comp.	ΔE (no CP)	ΔE (CP)	ΔE (no CP)	ΔE (CP)	ΔE (no CP)	ΔE (CP)
HF	**BD**	−16.42	−12.12	−13.59	−5.75	−12.48	−8.69
HF	**CD**	−15.95	−12.34	−14.28	−6.07	−12.70	−8.91
HF	**AE**	−16.11	−10.50	−15.63	−4.70	−14.82	−10.12
HF	**CE**	−13.59	−9.63	−12.08	−3.80	−10.53	−7.11
ClF	**BD**	−14.04	−8.47	−12.68	−1.62	−11.84	−8.30
ClF	**CD**	−13.00	−7.83	—[a]	—[a]	—[a]	—[a]
ClF	**AE**	−16.92	−10.39	−15.75	−1.71	−14.31	−9.94
ClF	**CE**	−12.07	−6.50	−12.47	0.28	−9.40	−6.37
HNC	**BD**	−15.38	−11.62	−17.04	−9.05	−17.55	−12.43
HNC	**CD**	−15.09	−11.73	−17.42	−9.46	−17.29	−12.35
HNC	**AE**	−12.05	−7.87	−14.70	−6.02	−15.62	−10.25
HNC	**CE**	−11.91	−8.88	−13.50	−6.46	−13.46	−9.03
HCN	**BD**	−14.37	−10.75	−14.42	−7.02	−15.11	−10.21
HCN	**CD**	−13.72	−10.56	−14.39	−7.10	—[a]	—[a]
HCN	**AE**	−9.51	−5.89	−11.05	−3.62	−11.60	−6.84

[a] These geometries spontaneously evolve to other ones.

Table 8 Cooperative effect energy (without and with BSSE correction by counterpoise method CP, kJ mol^{-1}) and interaction distances (Å) of the calculated complexes and variation of the interaction distances of trimers *vs.* dimers at MP2/aug-cc-pVTZ level

XY	Comp.	Coop-effect (no CP)[a]	Coop-effect (CP)[a]	d_1	d_2	Δd_1[b]	Δd_2[b]
HF	**BD**	−0.99	−0.79	2.917	2.045	−0.075	−0.036
HF	**CD**	−0.97	−0.67	2.926	1.997	−0.066	−0.036
HF	**AE**	−1.22	−0.90	3.088	1.992	−0.087	−0.028
HF	**CE**	−0.52	−0.29	3.073	1.991	−0.102	−0.042
ClF	**BD**	−0.24	−0.07	2.986	2.859	−0.044	−0.007
ClF	**CD**	—[c]	—[c]	—[c]	—[c]	—[c]	—[c]
ClF	**AE**	−0.48	−0.25	3.052	2.68	−0.02	−0.014
ClF	**CE**	−0.19	−0.05	3.069	2.814	−0.003	−0.021
HNC	**BD**	−1.69	−1.26	3.226	2.092	−0.1	−0.051
HNC	**CD**	−1.56	−1.13	3.198	2.039	−0.128	−0.05
HNC	**AE**	−1.38	−0.88	3.506	2.118	−0.187	−0.048
HNC	**CE**	−0.45	−0.01	3.443	2.038	−0.25	−0.051
HCN	**BD**	−0.99	−0.44	3.058	2.379	−0.081	−0.005
HCN	**CD**	—[c]	—[c]	—[c]	—[c]	—[c]	—[c]
HCN	**AE**	−0.90	−0.47	3.279	2.375	−0.089	−0.054

[a] Negative values mean greater stability of the trimer compared to the sum of energies of the isolated dimers. [b] Negative values mean shortening of the distance in the trimer compared to isolated dimer. [c] These geometries spontaneously evolve to other ones.

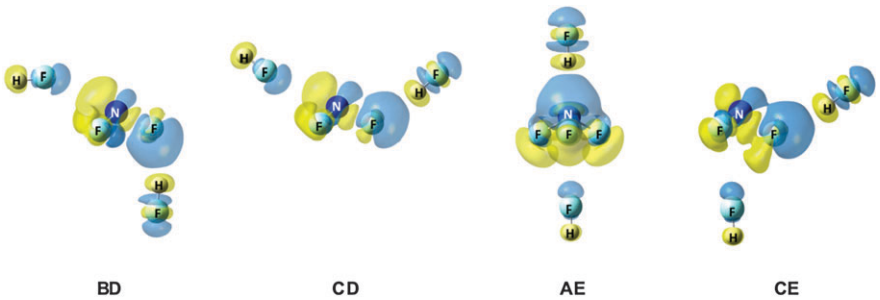

Fig. 6 Some examples of the electron density difference maps of HF : NF_3 : HF trimers located in this work. Blue and yellow isosurfaces represent gain and loss of electron density upon complexation respect to the isolated subunits. Contours shown are 0.0002 e per au calculated at the M05-2x/6-311++G(d,p) level.

seen, in all of the cases the distances observed within the dimers in the trimers are shorter than those of the corresponding isolated dimers, an indication of positive cooperativity.

Fig. 6 shows the electron density difference maps of the trimers of HF : NF_3 : HF. The trends are analogous to those observed for the dimers. Similar regions of gain or depletion of electronic charge found in dimers are observed and, as expected, in all the complexes the direction of the absolute charge displacement is $X_1Y_1 \rightarrow$ *NF_3 e-acceptor* $\rightarrow$ *NF_3 e-donor* $\rightarrow X_2Y_2$. As it can be seen, in the same way to that described for dimers, the largest increase of electron density occurs clearly in the *NF_3 e-donor* interaction area, than in the **D–E** ones.

Table 9 Electron density (au) of the trimers calculated at the M05-2x/6-311++G(d,p)

XY	Comp.	ρ_1	$\nabla^2\rho_1$	$\Delta\rho_1$[a]	ρ_2	$\nabla^2\rho_2$	$\Delta\rho_2$[a]
HF	**BD**	0.0079	0.0416	0.0005	0.0147	0.0695	0.0016
HF	**CD**	0.0067	0.0350	−0.0007	0.0157	0.0765	0.0011
HF	**AE**	0.0061	0.0313	0.0017	0.0209	0.0826	0.0019
HF	**CE**	0.0064	0.0326	0.0020	0.0161	0.0782	0.0015
ClF	**BD**	0.0063	0.0335	−0.0008	0.0115	0.0528	0.0010
ClF	**CD**	0.0060	0.0325	−0.0011	0.0123	0.0568	0.0009
ClF	**AE**	0.0055	0.0289	−0.0003	0.0187	0.0746	0.0009
ClF	**CE**	0.0063	0.0320	0.0005	0.0124	0.0572	0.0010
HNC	**BD**	0.0052	0.0185	0.0006	0.0120	0.0541	0.0014
HNC	**CD**	0.0054	0.0187	0.0008	0.0128	0.0586	0.0014
HNC	**AE**	0.0037	0.0146	0.0011	0.0139	0.0527	0.0014
HNC	**CE**	0.0037	0.0148	0.0011	0.0122	0.0564	0.0008
HCN	**BD**	0.0062	0.0258	0.0008	0.0084	0.0334	0.0012
HCN	**CD**	0.0064	0.0260	0.0010	0.0089	0.0367	0.0017
HCN	**AE**	0.0043	0.0187	0.0004	0.0087	0.0287	0.0010

[a] Positive values mean increase of the bcps' electron density of trimers compared to dimers.

Electron density analysis. The electron density characteristics of all the trimers considered have been analyzed according to the AIM theory. The AIM graphical analysis (Fig. 5) shows the same patterns of critical points found in dimers. In all the cases, bcps present small values of the electron density (ρ) and positive values of the Laplacian, an indication of closed shell interactions (Table 9). Regarding the dimers variation of the bcps' electron density ($\Delta\rho_1$ and $\Delta\rho_2$) within the trimers compared to that of the isolated dimers, an increase of electron density is in general observed. This is coherent with the increase of stabilization, what could be considered as a cooperativity indicator.

Natural bond orbital analysis. NBO analyses of charges of the trimers are gathered in Table 10. Despite compensation between donor/acceptor effects because of the dual behaviour of NF_3 in this type of complexes, the results in terms of absolute charges show a slight increment of the NF_3 charge in the trimers. It seems that the molecule of NF_3 donates more charge than it receives, maybe indicating that it is a better

Table 10 NBO and NEDA analysis of calculated trimers at the M05-2x/6-311++G(d,p) computational level

				Natural energy decomposition analysis (NEDA)/kJ mol^{-1}			
XY	Comp.	Charge transfer (e)[a]	$E2$/kJ mol^{-1}	CT	ES	POL	XT
HF	**BD**	0.007	12.01	−27.95	−15.73	−28.41	−19.16
HF	**CD**	0.007	15.77	−29.08	−15.02	−27.87	−17.28
HF	**AE**	0.018	23.47	−48.91	−17.36	−23.56	−21.21
HF	**CE**	0.007	16.11	−28.87	−12.84	−26.99	−18.79
ClF	**BD**	0.010	8.41	−29.25	−9.54	−39.33	−22.38
ClF	**CD**	0.009	10.63	−28.45	−9.92	−40.29	−21.59
ClF	**AE**	0.027	21.55	−50.21	−18.87	−47.07	−27.99
ClF	**CE**	0.010	10.54	−27.91	−9.29	−39.58	−21.97
HNC	**BD**	0.012	14.90	−32.38	−15.10	−18.12	−15.52
HNC	**CD**	0.012	18.70	−32.55	−16.15	−19.54	−15.82
HNC	**AE**	0.019	19.71	−40.71	−12.59	−12.97	−15.69
HNC	**CE**	0.010	16.99	−29.00	−11.13	−15.19	−13.26
HCN	**BD**	0.010	10.13	−31.76	−13.14	−26.23	−18.16
HCN	**CD**	0.009	12.22	−29.83	−13.56	−27.20	−18.03
HCN	**AE**	0.015	11.97	−31.88	−8.03	−15.48	−15.36

[a] Positive values mean charge transfer from NF_3 to the XY molecules in the complex.

Table 11 Cooperative effects based on the NBO/NEDA descriptors in both trimers and dimers

$D_{NBO}(X_1Y_1 : NF_3 : X_2Y_2) - D_{NBO}(X_1Y_1 : NF_3) - D_{NBO}(NF_3 : X_2Y_2)$

				Natural energy decomposition analysis (NEDA)/kJ mol^{-1}			
XY	Comp.	ΔCharge transfer (*e*)	Δ*E*2/kJ mol^{-1}	ΔCT	ΔES	ΔPOL	ΔXC
HF	**BD**	0.001	3.98	−4.82	−3.14	−4.52	−0.67
HF	**CD**	0.001	3.76	−4.82	−0.84	−3.27	0.63
HF	**AE**	0.002	4.18	−5.81	−4.97	−7.32	−4.35
HF	**CE**	0.001	4.10	−4.69	−3.76	−7.66	−3.56
ClF	**BD**	0.001	1.26	−1.01	−0.76	−4.35	−1.17
ClF	**CD**	0.001	1.43	−0.71	−0.51	−3.93	−1.00
ClF	**AE**	0.002	1.72	−2.63	−1.80	−2.26	−0.76
ClF	**CE**	0.001	1.34	−1.88	−1.55	−4.69	−1.30
HNC	**BD**	0.001	3.27	−4.09	−4.31	−4.44	−1.88
HNC	**CD**	0.002	3.80	−4.14	−4.57	−4.61	−1.68
HNC	**AE**	0.002	3.18	−4.85	−5.02	−4.27	−3.06
HNC	**CE**	0.001	2.09	−2.22	−3.98	−3.31	−1.76
HCN	**BD**	0.002	2.52	−5.07	−3.94	−5.10	−2.60
HCN	**CD**	0.002	3.56	−4.65	−4.40	−5.74	−2.43
HCN	**AE**	0.002	1.97	−2.26	−3.55	−3.09	−1.88

donor than acceptor. In addition, the second interaction established would be stronger because of the cooperative effects already discussed and this would deplete the NF_3 molecule of charge even further than in the dimer.

An orbital stabilization (*E*2) is observed in all the trimers (Table 10) always corresponding to the *NF_3 e-donor* fraction, showing the same patterns of orbital interaction described for the dimers [$LP_N \rightarrow$ BD* XY] in the interaction of type **A** or [$LP_F \rightarrow$ BD* XY] in the interactions of type **B** and **C**.

The NEDA results (Table 10) indicate that the influence of the charge transfer and polarization (CT and POL) is larger than the electrostatic component (ES), as observed and explained before for dimers. The CT component plays an important role especially in the complexes which have a type **A** interaction (trimers **AE**), whereas the polarization factor is significantly increased in complexes with ClF, because of the already mentioned polarizability of the chlorine atom.

The possible effect of cooperativity in terms of NBO/NEDA analysis has also been evaluated. Table 11 shows the differences of the absolute values of each NBO descriptor (D_{NBO}) in the trimers ($X_1Y_1 : NF_3 : X_2Y_2$) compared to the addition of the same descriptor in the corresponding two dimeric fractions ($X_1Y_1 : NF_3$ and $NF_3 : X_2Y_2$). All of the NBO descriptors indicate a positive cooperativity effect in the trimers. Thus, the value of NF_3 charge increases and there is an increase of stabilization by orbital interaction. Similarly, all components of NEDA in terms of attraction (CT, ES, POL, XT) have a negative value, indicating larger stabilization.

Conclusions

A theoretical study of the complexes formed between nitrogen trifluoride NF_3 and small ambidentate molecules such as HF, ClF, HNC and HCN has been carried out by means of DFT and *ab initio* computations. The dual character *e-donor*/*e-acceptor* of the NF_3 molecule has been evaluated both in the dimers and in the trimers. Five minimum configurations were found for each of the dimers, and four for the trimers.

In the case of the dimers, the most favourable interaction energies obtained with each of the ambidentate molecules range between −10 to −6 kJ mol^{-1}, whereas in the case of the trimers, more stable than the dimers as expected, the most favourable interaction energies appear to be between −17 to −10 kJ mol^{-1}, in all cases indicating the suitability of these complexes to be formed.

The AIM analysis of the electron density of these complexes shows that the bonds established among the monomers of these complexes are all close shell interactions. Regarding the dimers, in general, the interactions formed with HF are stronger than those with ClF and much stronger than those formed with HCN or HNC. In the case of the trimers, cooperativity effects are observed and, thus, the interactions in the trimers are stronger, in general, than those in the dimers as indicated by the larger values of electron density in the bcps.

An NBO analysis of all calculated complexes has been carried out. In all cases, an orbital stabilization (*E*2) is observed corresponding to the *NF_3 e-donor* fraction, showing similar patterns of orbital interaction for both the dimers and the trimers, that is [$LP_N \rightarrow$ BD* XY] in the interactions of type **A** or [$LP_F \rightarrow$ BD* XY] in the interactions of type **B** and **C**.

Finally, the NEDA study of all these complexes showed that the main stabilization terms are the charge transfer (CT) and polarization (POL) which are larger than the electrostatic component (ES). In the case of the trimers, all components (CT, ES, POL, XC) indicate a larger stabilization than for the dimers. The variation on the component that indicates deformation of the electronic clouds (DEF) in the NF_3 molecule is most pronounced in the systems that are more stable and especially in the dimers of type **A**. In the case of the trimers, the calculated value for NF_3 deformation increases due to its stronger interaction.

Summarizing, NF_3, considered as a greenhouse gas difficult to be eliminated from the atmosphere, is capable of strong binding to many different ambidentate molecules producing stable dimers and trimers; and maybe these molecules could be used as a trap to avoid NF_3 emissions.

Acknowledgements

This work was supported by the Ministerio de Ciencia e Innovación (Project No. CTQ2009-13129-C02-02) and

Comunidad Autónoma de Madrid (Project MADRISOLAR, ref. S-0505/PPQ/0225 and MADRISOLAR2, ref. S2009/PPQ-1533). Thanks are given to the CTI (CSIC) for allocation of computer time.

References

1 O. Ruff, J. Fischer and F. Luft, *Z. Anorg. Allg. Chem.*, 1928, **172**, 417–425.
2 (*a*) T. M. Klapötke, *J. Fluorine Chem.*, 2006, **127**, 679–687, and references therein; (*b*) C. J. Hoffman and R. G. Neville, *Chem. Rev.*, 1962, **62**, 1–18.
3 (*a*) P. B. Henderson and A. J. Woytek, *Nitrogen–nitrogen trifluoride*, in *Kirk–Othmer Encyclopedia of Chemical Technology, 11*, ed. J. I. Kroschwitz and M. Howe-Grant, John Wiley & Sons, New York, 4th edn, 1994, pp. 392–398; (*b*) F. Ishii and Y. Kita, in: *Advanced Inorganic Fluorides*, ed. T. Nakajima, B. Žemva and A. Tressaud, Elsevier, Amsterdam, 2000, ch. 19, p. 629; (*c*) D. T. Meshri, in *Advanced Inorganic Fluorides*, ed. T. Nakajima, B. Žemva and A. Tressaud, Elsevier, Amsterdam, 2000, ch. 20, p. 673.
4 R. F. Weiss, J. Muhle, P. K. Salameh and C. M. Harth, *Geophys. Res. Lett.*, 2008, **35**, L20821.
5 M. J. Prather and J. Hsu, *Geophys. Res. Lett.*, 2008, **35**, L12810.
6 (*a*) L. T. Molina, P. J. Wooldridge and M. J. Molina, *Geophys. Res. Lett.*, 1995, **22**, 1873–1876; (*b*) T. Wen-Tien, *J. Hazard. Mater.*, 2008, **159**, 257–263.
7 P. Antoniotti, S. Borocci and F. Grandinetti, *Eur. J. Inorg. Chem.*, 2004, 1125–1130.
8 A. Endou, T. W. Little, A. Yamada, K. Teraishi, M. Kubo, S. S. C. Ammal, A. Miyamoto, M. Kitajima and F. S. Ohuchi, *Surf. Sci.*, 2000, **445**, 243–248.
9 P. Antoniotti and F. Grandinetti, *Chem. Phys. Lett.*, 2002, **366**, 676–682.
10 R. Withnall and L. Andrews, *J. Phys. Chem.*, 1988, **92**, 2145–2149.
11 E. R. Waclawik, A. C. Legon and J. H. Holloway, *Chem. Phys. Lett.*, 1998, **295**, 289–297.
12 P. Antoniotti, L. Operti, R. Rabezzana, F. Turco and G. A. Vaglio, *Int. J. Mass Spectrom.*, 2006, **255–256**, 225–231.
13 K. Peia, J. Lianga and H. Lia, *J. Mol. Struct.*, 2004, **690**, 159–163.
14 (*a*) S. Borocci, N. Bronzolino, M. Giordani and F. Grandinetti, *Int. J. Mass Spectrom.*, 2006, **255–256**, 11–19; (*b*) F. Grandinetti and V. Vinciguerra, *THEOCHEM*, 2001, **574**, 185–193.
15 Y. Zhao, N. E. Schultz and D. G. Truhlar, *J. Chem. Theor. Comput.*, 2006, **2**, 364–382.
16 C. Møller and M. S. Plesset, *Phys. Rev.*, 1934, **46**, 618–622.
17 M. J. Frisch, J. A. Pople and J. S. Binkley, *J. Chem. Phys.*, 1984, **80**, 3265–3269.
18 (*a*) I. Alkorta, F. Blanco, J. Elguero, J. A. Dobado, S. Melchor Ferrer and I. Vidal, *J. Phys. Chem. A*, 2009, **113**(29), 8387–8393; (*b*) Y. Zhao, N. E. Schultz and D. G. Truhlar, *J. Chem. Theor. Comput.*, 2006, **2**(2), 364–382.
19 T. H. Dunning, *J. Chem. Phys.*, 1989, **90**, 1007–1023.
20 S. F. Boys and F. Bernardi, *Mol.Phys.*, 1970, **19**, 553–566.
21 R. F. W. Bader, *Atoms in Molecules: A Quantum Theory*, Clarendon Press, Oxford, 1990.
22 F. W. Biegler-König, R. F. W. Bader and T. H. Tang, *J. Comput. Chem.*, 1982, **3**, 317–328.
23 P. L. A. Popelier, with a contribution from R. G. A. Bone (UMIST, England, EU) MORPHY98, a topological analysis program; 0.2 ed., 1999.
24 I. Alkorta and O. Picazo, *ARKIVOC*, 2005, **ix**, 305–320.
25 A. E. Reed, L. A. Curtiss and F. Weinhold, *Chem. Rev.*, 1988, **88**, 899–926.
26 E. D. Glendening, K. Badenhoop, A. E. Reed, J. E. Carpenter, J. A. Bohmann, C. M. Morales and F. Weinhold, *NBO 5.0*, Theoretical Chemistry Institute, University of Wisconsin, Madison, 2001.
27 E. D. Glendening, *J. Am. Chem. Soc.*, 1996, **118**, 2473–2482.
28 GAMESS Version 11, M. W. Schmidt, K. K. Baldridge, J. A. Boatz, S. T. Elbert, M. S. Gordon, J. H. Jensen, S. Koseki, N. Matsunaga, K. A. Nguyen, S. J. Su, T. L. Windus, M. Dupuis and J. A. Montgomery, *J. Comput. Chem.*, 1993, **14**, 1347–1363.
29 J. Sheridan and W. Gordy, *Phys. Rev.*, 1950, **79**, 513–515.
30 S. N. Ghosh, T. Ralph and G. Walter, *J. Chem. Phys.*, 1953, **21**, 308–310.
31 I. Alkorta, I. Rozas and J. Elguero, *J. Org. Chem.*, 1997, **62**, 4687–4691.
32 (*a*) T. Clark, M. Hennemann, J. S. Murray and P. Politzer, *J. Mol. Model*, 2007, **13**, 291–296; (*b*) J. S. Murray, P. Lane and P. Politzer, *Int. J. Quantum Chem.*, 2007, **107**, 2286–2292; (*c*) P. Politzer, J. S. Murray and P. Lane, *Int. J. Quantum Chem.*, 2007, **107**, 3046–3052; (*d*) J. S. Murray, P. Lane and P. Politzer, *Int. J. Quantum Chem.*, 2008, **108**, 2770–2781.
33 (*a*) J. J. Fisher and T. B. McMahon, *J. Am. Chem. Soc.*, 1988, **110**, 7599–7604; (*b*) F. Grandinetti, J. Hrušák, D. Schröder, S. Karrass and H. Schwarz, *J. Am. Chem. Soc.*, 1992, **114**, 2806–2810.
34 E. P. L. Hunter and S. G. Lias, *J. Phys. Chem. Ref. Data*, 1998, **27**, 413–656.
35 T. B. McMahon and P. Kebarle, *J. Am. Chem. Soc.*, 1985, **107**, 2612–2617.
36 I. Alkorta, I. Rozas and J. Elguero, *Chem. Soc. Rev.*, 1998, **27**, 163–170.
37 R. G. A. Bone and R. F. W. Bader, *J. Phys. Chem.*, 1996, **100**, 10892–10911.
38 O. Picazo, I. Alkorta and J. Elguero, *J. Org. Chem.*, 2003, **68**, 7485–7489.
39 I. Mata, I. Alkorta, E. Molins and E. Espinosa, *Chem.–Eur. J.*, 2010, **16**, 2442–2452.